Tribology International 119 (2018) 270–280

Contents lists available at ScienceDirect

Tribology International

journal homepage: www.elsevier.com/locate/triboint

Generation of Acoustic Emission from the running-in and subsequent micropitting of a mixed-elastohydrodynamic contact

S. Hutt, A. Clarke *, H.P. Evans

School of Engineering, Cardiff University, Cardiff, United Kingdom

ARTICLE INFO

Keywords:
Acoustic Emission
Running-in
Micropitting
Mixed lubrication

ABSTRACT

This paper presents the use of Acoustic Emission to study the running-in and subsequent micropitting of a pair of hardened steel surfaces under mixed lubrication conditions. These surfaces were loaded together under rolling/sliding conditions typical of heavily loaded gearing. Relocation profilometry was used to measure the rapid running-in process and the development of micropits. Acoustic emission (AE) was found to be highly sensitive to both the initial changes in surface topography during the running-in process, and to subsequent changes caused by micropit formation. However, AE appears to be sensitive to changes in asperity interaction rather than the underlying mechanisms of plastic deformation, crack growth and fracture. It is concluded that AE can provide considerable insight into conditions in mixed-elastohydrodynamic contacts.

1. Introduction

There is currently considerable interest in using Acoustic Emission to monitor tribological conditions in mechanical equipment, such as gears and bearings within aerospace and renewable energy power transmissions. AE is the release of ultrasonic stress waves within a material, caused by energy release from sources such as plastic deformation, crack growth, frictional contacts and fluid cavitation.

AE is widely held to be a sensitive technique which offers significant advantages in terms of early fault detection and diagnosis when compared to other monitoring methods [1,2]. Although not as well established when compared to vibration or temperature-based techniques, it has been used effectively at least in laboratory conditions to detect faults in rolling element bearings [3–5]; to study the piston ring/liner interface in diesel engines [6]; and extensively for studies of tribological conditions in wear or contact fatigue testing [7–10].

Various workers have investigated the use of AE to monitor gear systems. Toutountzakis et al. [11] presented tests using spur gears which demonstrated the effects of operating conditions on AE, and also the ability of AE to detect changes in tooth surface condition. They subsequently undertook a series of experiments using seeded, or artificial, pitting defects on spur gears [12]. They concluded that seeded defects introduced different source mechanisms when compared to naturally-occurring defects, and recommended the use of life tests where defects are allowed to occur naturally to develop the use of AE for gear monitoring. Within a gearbox, transmission paths between source (at the tooth contact) and sensor (perhaps mounted on a bearing housing for example) may be complex with multiple interfaces and complex attenuation behaviour. Sing et al. [13] studied these complex transmission paths using a tooth breakage test rig, whilst Crivelli et al. [14] investigated the use of advanced signal processing methods to detect AE from tooth fatigue cracking in the root fillet region. In life tests of precision forged gears, Scheer et al. [15] used wavelet-based techniques to detect signals related to micropitting and to tooth root fatigue, whilst Wirtz et al. [16] adopted similar signal processing techniques to identify micropitting in an FZG back-to-back gear test rig, with sensors mounted on the gear test housings.

Barrueto Novoa and Molina Vicuna [17] reviewed the various hypotheses relating to the sources of AE in gears. Typical AE signals measured for spur gears consist of continuous emission, superimposed with a series of transient bursts spaced at the gear meshing frequency. They considered that the transient bursts could be caused by the instantaneous pure rolling conditions at the pitch point, or by the EHL exit pressure spike, or (as seems most likely) the shock loading caused by tooth engagement, whilst the continuous emission was most likely related to asperity contact. They conducted tests using a planetary gearbox [17,18] where the effects of load, speed and lubricant temperature were investigated, concluding that temperature and speed-related changes in the lubricant film thickness between the gears affected the levels of asperity interaction during the meshing cycle and, hence, the

* Corresponding author.
E-mail address: clarkea7@cardiff.ac.uk (A. Clarke).

https://doi.org/10.1016/j.triboint.2017.11.011
Received 27 July 2017; Received in revised form 23 October 2017; Accepted 7 November 2017
Available online 8 November 2017

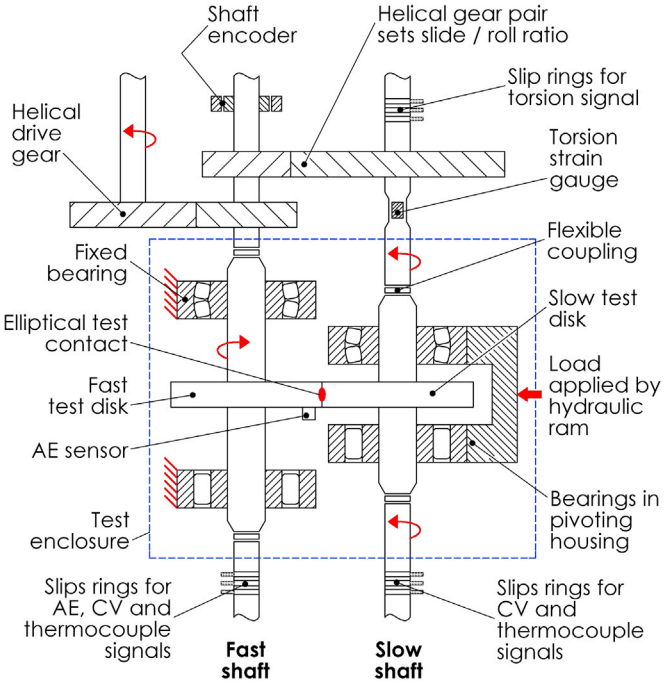

Fig. 1. Schematic of the twin disk rig.

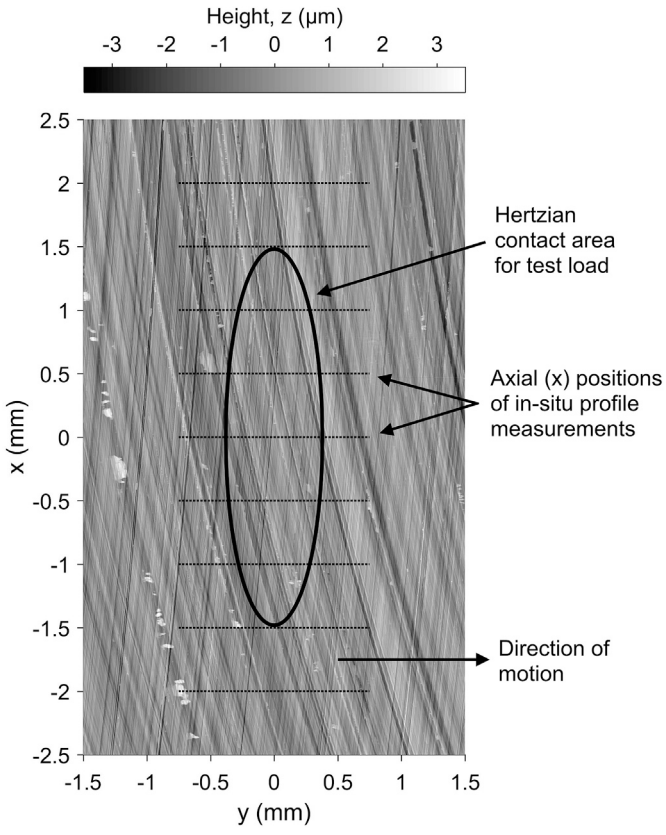

Fig. 2. The composite surface roughness of the disks before testing. Also shown are the Hertzian contact area for the test load and the axial positions for the in-situ roughness measurements made during testing.

levels of AE produced. To investigate the link between specific film thickness (or lambda ratio) and AE, Rajah Hamzah and Mba [19] conducted a series of novel experiments where short bursts of liquid nitrogen were used to rapidly cool the gear surface, with the aim of increasing lubricant viscosity by a significant amount. They found a reduction in RMS levels of AE, which directly followed the changes in gear temperature, suggesting a strong link between specific film thickness (and therefore asperity interaction) and AE. This was confirmed by further experiments using spur and helical gears under a range of operating conditions [20], where they concluded that, at least in part, asperity interaction was responsible for the AE from running gears. Other work [21,22] also identified asperity interactions under the mixed lubrication conditions which occur in heavily loaded gearing to be a source of AE signals.

This paper presents experimental work which is part of a wider study by the authors to investigate AE caused by asperity interactions in mixed lubrication conditions, using a power-recirculating twin disk test rig. This approach has many advantages as it allows the scientific study of this AE source without the complications of the variable kinematic and loading conditions within the gear meshing cycle, or the other potential sources of AE such as tooth engagement. In this paper, AE is found to be sensitive to subtle changes in asperity geometry, quantified using in-situ relocation profilometry, due to running-in and subsequent micropitting of the steel disk surfaces.

2. Twin disk test rig

The experiment was carried out on a twin disk rig used to simulate, with simplified kinematics, the contact between heavily loaded gears. It has been previously used to investigate how material hardness, and the lubrication regime, i.e. the specific film thickness, affect the surface wear and the contact friction [23,24]. It has also been used to evaluate novel techniques for investigating the lubrication regime, such as electrical resistance of the lubricant film [24], and currently, acoustic emission measurements.

Fig. 1 shows a schematic of the rig. The test contact is made between two geometrically identical disks mounted on shafts connected by a helical gear pair, the ratio of which determines the slide/roll ratio (SRR) of the disk contact. A constant SRR, as generated by this rig, differs from that of meshing gear teeth, where it varies over the tooth contact cycle; however, it significantly reduces the complexity of the measurement and analysis techniques required to study the contact.

In order to investigate the possibility of very rapid wear and surface modification regimes, occurring in the order of ones or tens of fast disk cycles, it is necessary to minimise transients associated with starting and stopping a test. This is achieved by the use of a hydraulic ram which provides a rapid loading and unloading response. The slow shaft is supported in a pivoting housing that allows the centres-distance of the disks to vary in response to the load. A flexible coupling arrangement ensures the fast and slow shaft remain parallel. When no load is applied the disks do not make contact which allows the rig to be run up to speed before the test is started. The contact load, which is directly measured by a load cell, is calibrated prior to testing by adjustment of the hydraulic pressure supplied to the ram. During calibration a wedge is placed in-between the fast and slow shafts to keep the disks separated. A ball-valve is used to quickly switch the ram pressure on and off at the start and end of a test.

The test disks are made of a case hardened gear steel meeting Rolls-Royce specification 6010. The disks have a diameter of 76.2 mm, a face width of 9.5 mm and a crown of radius 304.8 mm. This geometry results in a spheroidal contact face that generates an elliptical test contact having a 4 to 1 aspect ratio. The minor axis of the ellipse is aligned in the slide/roll direction. The crown is machined using a special grinding technique that results in a surface with the ridges and valleys aligned approximately normal to the slide/roll direction. This closely replicates the roughness orientation found in ground gear teeth. Further details of the steel specification and grinding process are given in Ref. [25].

For the work presented in this paper a single set of previously un-used disks was tested. The Vickers hardness of each disk was tested and found

Table 1
Rig and contact parameters.

Slide/roll ratio, [Gear ratio]	0.5, [5/3]
Fast disk Speed (rpm)	1000
Mean Entrainment velocity (m/s)	3.2
Load (N)	1460
Maximum Hertzian contact pressure (GPa)	1.2
Hertzian contact dimensions (mm)	0.8 × 3.0
Oil bath temperature (°C)	80

to be 760 Hv for each. Before the disks were assembled in the rig the roughness of a small area from the contact face of each was measured using a Taylor Hobson Talysurf Form2 stylus profilometer. Fig. 2 shows the composite roughness (the sum of the roughness of each disk) made using these measurements. The grinding process produces ridges and valleys that are 'extruded' across the disk width along a slightly swept path. When assembled in the rig the direction of roughness sweep for one disk is opposed to that of the other thus generating the cross-hatched composite roughness evident in Fig. 2.

The contact is lubricated by an extreme pressure gear oil conforming to Defence Standard OEP-80 [26]. The oil is pumped from a heated bath and sprayed directly onto the inlet and outlet of the test contact to ensure it is always flooded. Oil from the same bath is also used to lubricate the drive gears and support bearings. The rig is driven by a three phase electric motor controlled by a variable frequency drive, and geared to provide fast shaft speeds between 200 and 2000 rpm. An encoder on the fast shaft measures its speed, counts the number of cycles and synchronises the data acquisition system. The temperature of each disk is measured using an embedded thermocouple located in a small hole 3 mm below its contact surface on the centre line. A strain gauge on a reduced diameter section of the slow shaft measures the torsion between its driven gear and the test disk, this can be used to estimate the friction at the contact, and is calibrated to isolate the frictional traction at the contact from parasitic friction losses in the bearings and shaft windage.

The amount of direct asperity interaction at the contact is monitored by measurement of its electrical resistance. To facilitate this the section of slow shaft supporting its test disk is electrically isolated from the main body of the rig. This allows an electrical potential, termed here the Contact Voltage (CV), to be set up and measured across the disks. The contact resistance varies with the amount of direct, metal to metal, asperity contact that bridges the oil film. In full film lubrication the contact resistance is effectively infinite and the CV will be at a maximum that is equal to the source potential. In mixed lubrication the instantaneous CV will fluctuate rapidly with the amount of instantaneous asperity contact. The mean CV, over time, will give an indication of where in the mixed lubrication spectrum the contact is operating. In boundary lubrication the contact resistance is effectively zero and thus the CV will measure zero. A detailed study of CV measurements in mixed lubrication has been previously carried-out using the twin disk rig and is presented in Ref. [24], together with a more detailed description of the contact voltage measurement technique. For the tests presented in this paper a 44 mV potential was used. For clarity the CV results are presented normalised between zero, the minimum, and one, the maximum representing full film conditions.

A Physical Acoustics Pico transducer is used to measure the AE from the contact. It has a nominal operating range of 200–750 kHz and resonant frequency of 250 kHz. This sensor was chosen primarily for its small size and ease of installation in the test rig. The sensor is clamped to the side of the fast disk near its periphery. A thin film of silicone sealant is used as an acoustic couplant between the sensor and disk face to aid signal transmission across the interface. This material is widely used within the AE research community as an effective acoustic couplant [5]. Moreover, the silicone layer is extremely thin, as primary mounting of the sensor is achieved using a clamp. The transducer signal is routed through an air cooled silver/graphite slip ring to a 40 dB pre-amplifier with a 20 kHz high-pass filter. A second Pico transducer is affixed to one of the fast shaft bearing housings. For this, the signal attenuation is sufficient to ensure that AE from the test contact is negligible. Thus data from this sensor can be used to help to identify sources of noise. A dedicated Physical Acoustics computer performs analogue to digital conversion on the amplified signals from both sensors and saves them when triggered by a signal from the rig computer.

3. Test parameters and procedure

The experiment consisted of a number of 'test stages' in-between which the rig was stopped so that the disk surfaces could be measured and changes to their roughness monitored. Constant and identical control parameters were used for all test stages, and are shown in Table 1. They were chosen, based on previous experience, to give a specific film thickness corresponding to mixed lubrication conditions that would cause micro-pitting fatigue within the time available for testing.

The only variation between the test stages was their duration. It was intended to run-in the disks in a single, initial, stage, the duration of which was set at 3 min based on previous running-in experiments using similar disks and contact parameters [23]. The length of subsequent stages was decided as the test progressed based upon the rate of surface modification. The schedule that resulted is shown in Table 2.

To minimise the effect of temperature transients at the start of each running-stage, the unloaded disks were first run (out of contact) at the test speed whilst the oil was heated and pumped through the test enclosure. This allowed it to approach thermal equilibrium, usually after a few hours, before the test stage was started by the application of the load, bringing the disks into contact.

The data acquisition was synchronised with the fast disk by a single shaft encoder pulse per rotation. Upon each pulse the load, temperatures and CV were sampled at 1.25 MHz for 75% of a single fast disk rotation, these data were then averaged to provide a single mean value for each fast disk rotation. (Only 75% of each rotation could be sampled due to the triggering method used). The acquisition of the AE signal was different dependant on the length of the test-stage. For the first two short stages it was continuous, with sampling started shortly before the load was applied and stopped after it was removed. For the remaining stages it was synchronised with the fast disk and only periodically triggered as follows: For stages 3–13 every 100^{th} fast disk rotation, and for stages 14–19 every 500^{th}. The sample period was chosen to be 5 fast disk rotations as the composite surface roughness repeats every five fast disk rotations, (the gear ratio was 5/3, that is, three slow disk rotations per five of the fast disk). All AE acquisition was at a sample rate of 2 MHz.

The surface measurements of the disks, made in-between each test stage and at the start and end of the experiment, were carried out in-situ using a portable Taylor Hobson 2D profilometer, using a stylus with a 90° conical diamond tip with a 2 μm radius. Use of an in-situ technique allowed preservation of the disks' relative angular orientation throughout

Table 2
Running schedule.

Test Stage/s	Desciption	Duration per stage (min)	Fast disk cycles per stage	Cumulative fast disk cycles at end of stage/s
1	Run-in	3	3000	3000
2	Run-in validation	3	3000	6000
3 to 13	Fatigue testing	100	1×10^5	$\sim 10 \times 10^5$
14 to 19	Fatigue testing	300	3×10^5	$\sim 25 \times 10^5$

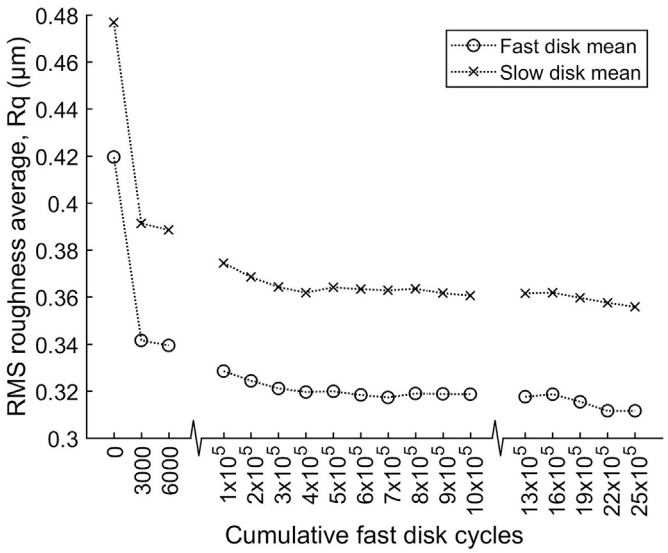

Fig. 3. The RMS roughness, R_q, from the contact path of each disk vs cumulative fast disk cycles. The values have been calculated using all five profiles within the contact path (see Fig. 2). The scale of the horizontal axis is not uniform, two breaks indicate where the scale changes.

the entire experiment. This was important as each specific orientation generates a specific composite roughness which will run-in and wear as its topography dictates. If that topography suddenly changed due to a new orientation it would initiate a new running-in and wear phase as new asperity interactions occur.

The in-situ disk profiles were measured in the circumferential direction, i.e. across the lay of the ridges and valleys, normal to the cylindrical axis of the test disk/shaft. It is useful to study how representative sections of surface roughness change as test progresses for which positional reference points were required. Score marks on the side of the disks were used as a coarse reference for circumferential position. These did not need to be precise as cross-correlation techniques were used to accurately re-align the profiles after measurement. The profilometer cannot be left in place whilst the rig is running so the side of the disk was used as a reference point for all axial measurements. The profilometer is mounted on an axial linear stage whose position is measured by a dial gauge. The position of the side of the disk was established as follows: The profilometer stylus was positioned by eye on the crest of the disk. It was then moved axially outwards using the linear stage until its height decreased by 60 µm, this indicated the edge of the disk. The error in axial positioning was likely to be at least ±5 µm dominated by the resolution of the dial gauge and error in locating the disk edge.

For this experiment 12 mm long profiles were measured at a single circumferential position and nine axial positions per disk. The axial measurement positions relative to the disk centre line are shown in Fig. 2. The measurements were spaced, in 0.5 mm increments, over a 4 mm range centred on the disk centre line. Given the nominal axial width of the contact, approximately 3 mm, this resulted in 5 profiles within the contact path, two at its nominal edge and two outside the contact area.

4. Evolution of surface topography during tests

This section describes the changes to the contact surfaces that occurred over the course of the experiment. As discussed in the test procedure, the surface measurement schedule was not fixed at the start but was determined as the test progressed. The RMS roughness (R_q) was used to confirm nominal end of the running-in process and the start of steady state fatigue testing. The change in R_q, for each disk, over the test is shown in Fig. 3. As expected, running-in caused a rapid and large reduction in the R_q of both disks. For the first 6000 fast disk cycles, 97% of the reduction occurred within the first 3000 cycles and only 3% in the subsequent 3000 cycles. This indicates that by the 6000th cycle, (the end of the second test stage), the surfaces were at a comparatively steady state and thus were fully run-in, in agreement with previous work on surface topography changes during running-in Ref. [23]. Comparison of relocated profiles confirmed the stability of the surfaces at 6000 cycles. Subsequently, over the course of the fatigue test, there was a further, much slower, decrease in R_q, however approximately 70% of the total decrease for the entire test occurred within the first 3000 cycles.

Fig. 3, which has a displaced zero, may give the impression that the slow disk was generally rougher than the fast however this difference is not significant and is likely to be due to circumferential variation, and within the manufacturing tolerance applied to surface finish. On average, over the entire circumference, the disks are of similar roughness. The relative changes to the R_q of each disk were similar despite their different starting values, with no signs of convergence. This is likely because the R_q

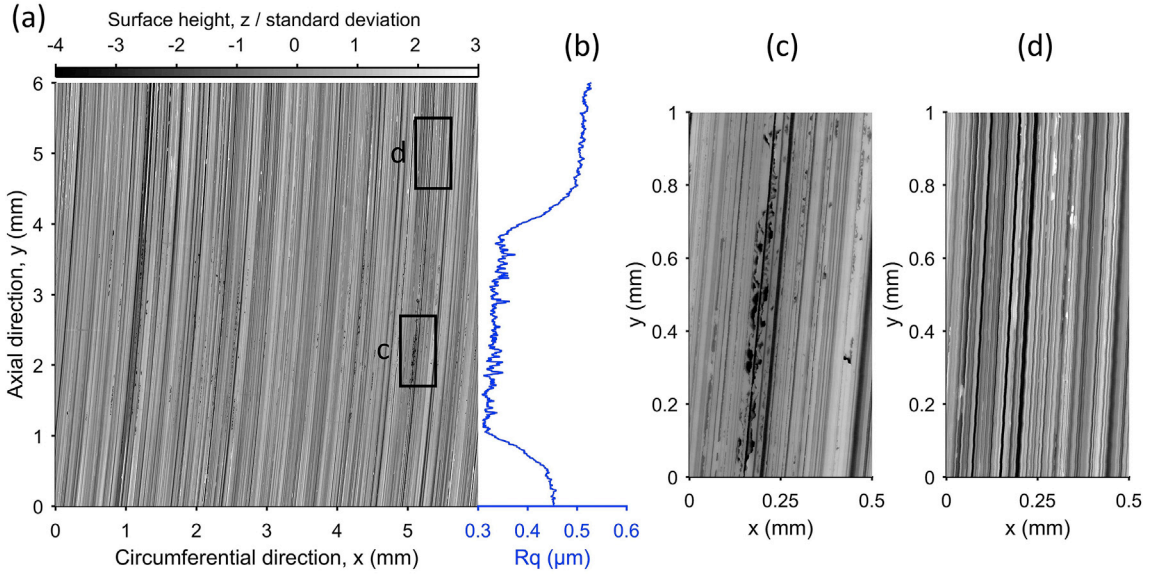

Fig. 4. a) High resolution roughness measurement of the fast disk at the end of the test. b) RMS roughness vs axial (y) position. c) Close-up of an area on the contact path showing a prominent series of micro-pits, visible as dark speckles, aligned with the ridges. d) Close-up of an area outside the contact path for comparison.

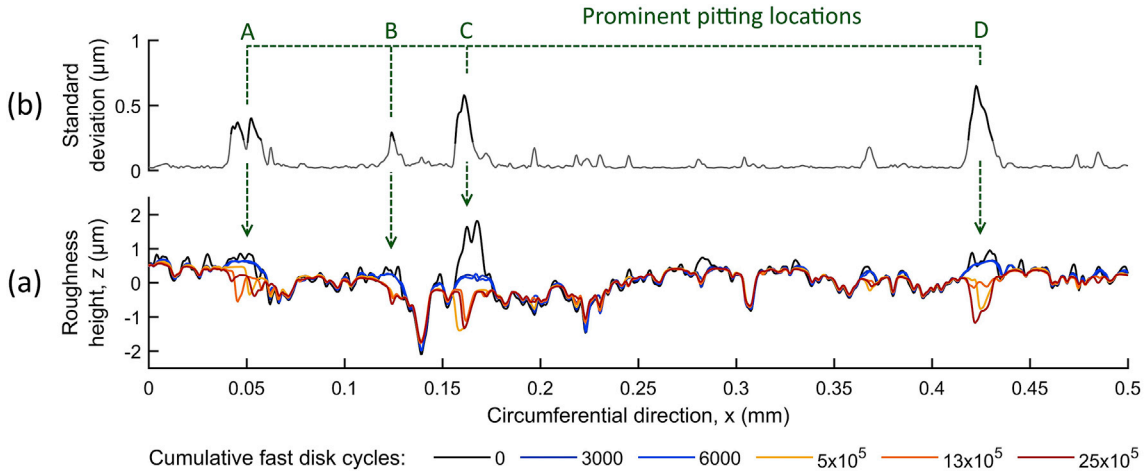

Fig. 5. An example of micro-pitting identification using a 0.5 mm profile length from the fast disk centre-line. (a) A selection of realigned profiles showing the surface in the following conditions: un-run (black), run-in (blue), and pitted (yellow to red). (b) The standard deviation of realigned profiles measured between 6000 and 25 × 10^5 fast disk cycles is shown above.

represents profile features at all heights whereas surface modification predominantly affects asperity tips. Thus unless there is significant wear there will always be a constant component of the R_q that is dependent on the local valley features.

Although the Rq data provides an indication of the relative rate of surface modification it does not offer any insight into the type of modification, i.e. the wear mechanism. To characterise this more sophisticated measurements and analysis are required. Fig. 4(a) presents a high resolution areal roughness measurement of a 6 × 6 mm area of the fast disk, measured at the end of the test. This area covers the entire width of the contact path and some of the un-run regions on either side. The location of the contact path can be determined by consideration of the variation of R_q with axial position as plotted in Fig. 4(b). The region with low R_q values, (between 0.3 and 0.4 μm), identifies the contact path. It has a width of just under 3 mm which is close to that expected from a Hertzian contact calculation. At both edges of the contact there is a region, approximately 0.5 mm wide, where the Rq smoothly transitions between that of the contact path and that of the un-run regions. The areal roughness measurement shows explicitly that micro-pitting had occurred by the end of the test. The micro-pits are evident as dark specks within the contact path. They are not evenly distributed across the surface but tend to be clustered along prominent asperity ridges. Fig. 4(c), an enlarged view of a region within the contact path, shows an asperity ridge having a set of particularly numerous and large micro-pits. For comparison Fig. 4(d) shows a section of the same ridge located outside the contact path. The section within the contact path would have looked like this at the start of the test. An equivalent measurement of the slow disk showed that micropitting had also occurred on this disk by the end of the test.

As shown by Fig. 4, micro-pits can be identified easily using areal (three-dimensional) roughness measurements. However as the twin disk rig is not currently equipped to make in-situ three-dimensional measurements it is not possible to use these to identify when these pits are formed and how they grow. Knowledge of this is required to assess if micro-pitting has AE characteristics distinct from that of other wear mechanisms, and this was assessed statistically using the two-dimensional in-situ profiles. Roughness profiles made at different times were precisely aligned using cross-correlation in the circumferential direction, and by minimising the mean height difference between deep valley features in the vertical direction. The mean line cannot be used as height reference as it changes due to wear of surface asperities whereas the deep valley features are assumed to be unaffected by wear.

Fig. 5 (a) presents an example of the aligned profiles for a short length of the fast disk centre-line. In this figure, profiles measured at different stages in the test from un-run (black), to immediately after running-in (blue) and during the fatigue testing (yellow to red) are overlaid. This allows the effects of different surface modification mechanisms to be easily visually identified and distinguished from one another. It can be seen that the running-in process (black to blue) resulted in the flattening and rounding of numerous asperities, large and small. Much of this is suspected to be due to plastic deformation [23], however for the most prominent asperities the local material volume appears to reduce which implies some material removal as well. An example of the apparent reduction in volume can be seen at C. By the end of the experiment, many of the locations where running-in had caused the most initial change had subsequently pitted. Examples of this are at positions A to D. It can be seen that these micro-pits have dimensions on the scale of the previously existing roughness features. Thus it is not possible to identify micro-pits from 2D analysis without considering the surface change over time, i.e. the aligned profiles. Once a pit is identified it might be supposed that it would be a simple matter to track its growth by considering the change from one measurement time to the next. Unfortunately, this is not the case. The error in the axial position of the profile measurements is on the same scale as the width of a typical micro-pit so it cannot be assumed that a pit is consistently measured in the same location. This will cause the pit size to fluctuate based on how close the edge or centre it was measured. An example of this can be seen at D where the pit measured after 13 × 10^5 cycles appears shallower than that measured after 5 × 10^5 cycles. Whilst the disks were cleaned before each measurement, debris trapped within valley features may also affect the measurements.

Visual examination of the aligned profiles cannot accurately gauge the rate of pit formation and growth and so a mathematical method has been developed instead. This requires the identification of all sections of the profile that had pitted by the end of the test. The standard deviation of the set of aligned profiles at each circumferential position is used to identify pitted locations, an example of this is shown in Fig. 5(b). For this the standard deviation, at each circumferential sample point, has been calculated for all profiles measured after running-in (from cycle 6000 onwards). The standard deviation is comparatively high at pitting locations for two reasons: firstly the growth of the pit over time, and secondly, the axial position error has a greater affect at these locations. A minimum standard deviation threshold is used to identify the final pitting locations. In Fig. 5(b), a threshold of 0.2 μm, shown in bold, has been used to identify pits A to D.

The rate of pit formation and growth was assessed by consideration of how the mean height of the identified final pitting locations changed over the test. This is shown in Fig. 6 for each disk separately, with the mean height of the entire profile and the un-pitted locations shown for comparison. The five axial profile positions within the contact path were analysed giving a total sample length of approximately 54 mm. The end

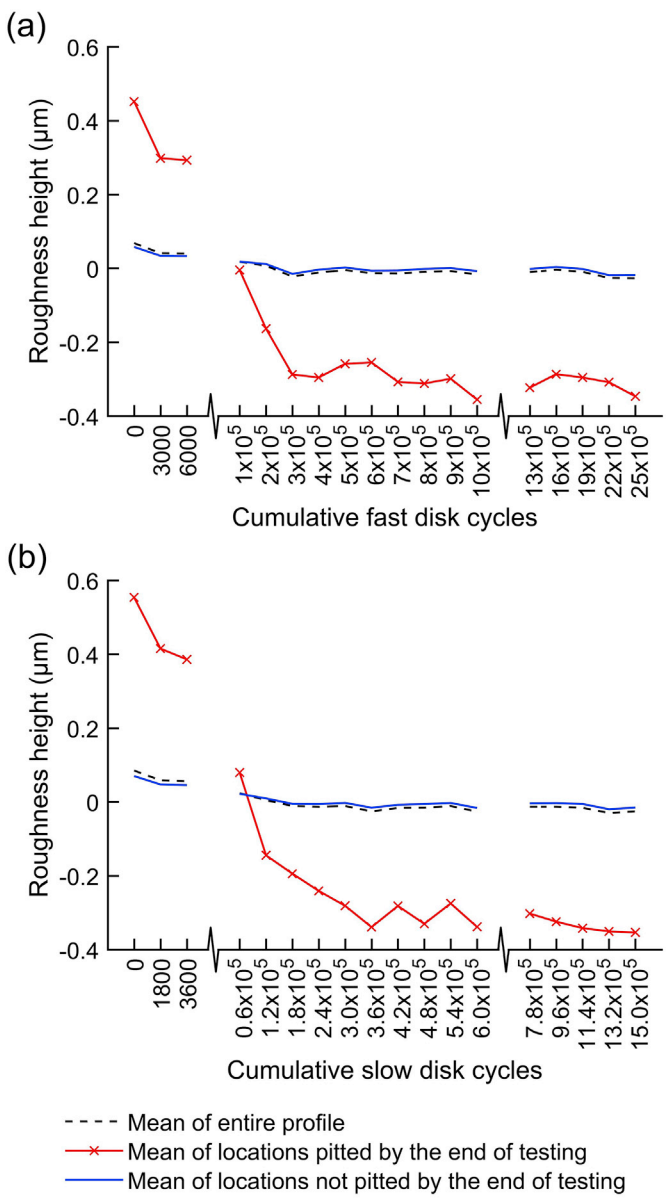

Fig. 6. Comparison of the change in mean roughness height for locations that had pitted by the end of the test and those that had not. Calculated using the five axial profile positions within the contact path for a) the fast disk and b) the slow.

pitting locations were calculated using a standard deviation threshold of 0.2 μm. This gives the percentage of the profile that was pitted as 2.6% for the fast disk and 3.1% for the slow. However, these are almost certainly underestimations as it can be seen in Fig. 5(b) that a threshold of 0.2 μm excludes the edges of the large pits and some small pits entirely. Despite this, a value of 0.2 was found to represent a good compromise between noise induced by a small sample size, prone at a high threshold, and erroneous pit identification, prone at a low threshold. From Fig. 6 it can be seen that, at the start of the test, locations that subsequently pitted were, unsurprisingly, at relatively high elevations. Running-in caused a moderate reduction in their mean elevation. However the most substantial decrease, and the change from a positive to negative mean elevation, occurred in the early stages of the fatigue test, between 6000 and 2×10^5 fast disk cycles (test stages 3 and 4). This indicates that the majority of the pitting took place in this period. By about a quarter of the way through the fatigue test the mean elevation of the pitting locations appears to have stabilised at a minimum for both disks. This implies that, for these test conditions micro-pitting was a self-limited wear process. The likely explanation for this is as follows: Initially the contact load is carried by a few prominent and heavily loaded asperities. As these are removed by micro-pitting the load is redistributed more evenly to other asperities and the partial lubricant film, until the cyclic loads on individual asperities are not sufficient to cause fatigue failure.

5. Running-in

In this section the AE and CV measurements made during the running-in process are assessed with reference to the measured surface changes discussed in section 4. Fig. 7 shows the measurements made during test stage one, running-in, and test stage two, validation of the run-in state. As discussed in the test procedure, the AE for these was acquired continuously as a broadband signal which does not lend itself to easy interpretation. Frequency filtering and time averaging were required to produce useful results. The technique used here was to calculate the discrete Fourier transform (DFT) along a moving window, the width and increment of which was used to control the amount of time averaging. This gave a three dimensional data set of time vs frequency vs amplitude (An example of a data set of this type is presented in Fig. 11). This allowed for easy filtering by directly extracting a subset of the frequency axis. The absolute mean within this subset was then calculated to give the 'mean AE' vs time. For the AE results presented in Fig. 7 the window width was equal to the time period required for the composite roughness to repeat, 0.3 s, and the frequency range was 150 kHz–300 kHz. This frequency range, which has been used for all the 'mean AE' results in this paper, was chosen as it offers the best signal to noise ratio. This range was identified by comparing the spectral distribution of data from the fast disk transducer with that from the bearing housing transducer. The spectral distributions are presented and discussed later in the paper.

Fig. 7 shows that when the disks were first loaded at the start of the running-in, (A), there was an extremely short transient peak in the AE to above 1.5 mV. After this it remains at a comparatively steady state of approximately 0.9 mV until the end of the first stage (B). It is known that there was a large reduction in the surface roughness during this period so a large reduction in AE is also expected. The only reduction occurring is the decay from the transient peak which is extremely rapid, effectively instantaneous on the time scale of the entire test stage. This suggests that running-in occurred almost instantly upon the start of the test, which is in agreement with previous work which suggests that initial running-in is predominantly a process of plastic-deformation [23,27]. Subsequent modification of the surface geometry is predominantly due to micro-pitting rather than further running-in. This may be confirmed by examination of non-pitted regions of the profiles in Fig. 5, which show that there is very close agreement between profiles taken after the running-in stage and those taken at the end of the test. Further evidence of this is provided by consideration of the AE response at the start of the second test-stage (C). The decrease in surface roughness for this test stage was negligible compared to that in the first. If the transient AE peak is due to running-in it should therefore be absent, or greatly diminished, and the latter is the case.

In the second stage there is a short smooth increase in the AE after the transient before it approaches steady state. This is due to the temperature change which affects the AE indirectly. Fig. 7 shows that upon initial loading, the temperature of both disks immediately starts to increase. This is due to frictional heating at the contact. The heating is relatively minor and is consistent throughout the test so a new thermal equilibrium is quickly approached. The effect of an increase in temperature is to lower the viscosity of the oil film in the contact and consequently decrease its thickness [24]. This leads to greater direct asperity contact which results in an increase in AE [22]. Fig. 7 shows the temperature response for both test stages to be similar however the expected increase in the AE is only evident in the second. This is attributed to the effects of running-in (reducing asperity interaction) masking the counter-effects of increased temperature (thinning films leading to increased asperity interaction) in

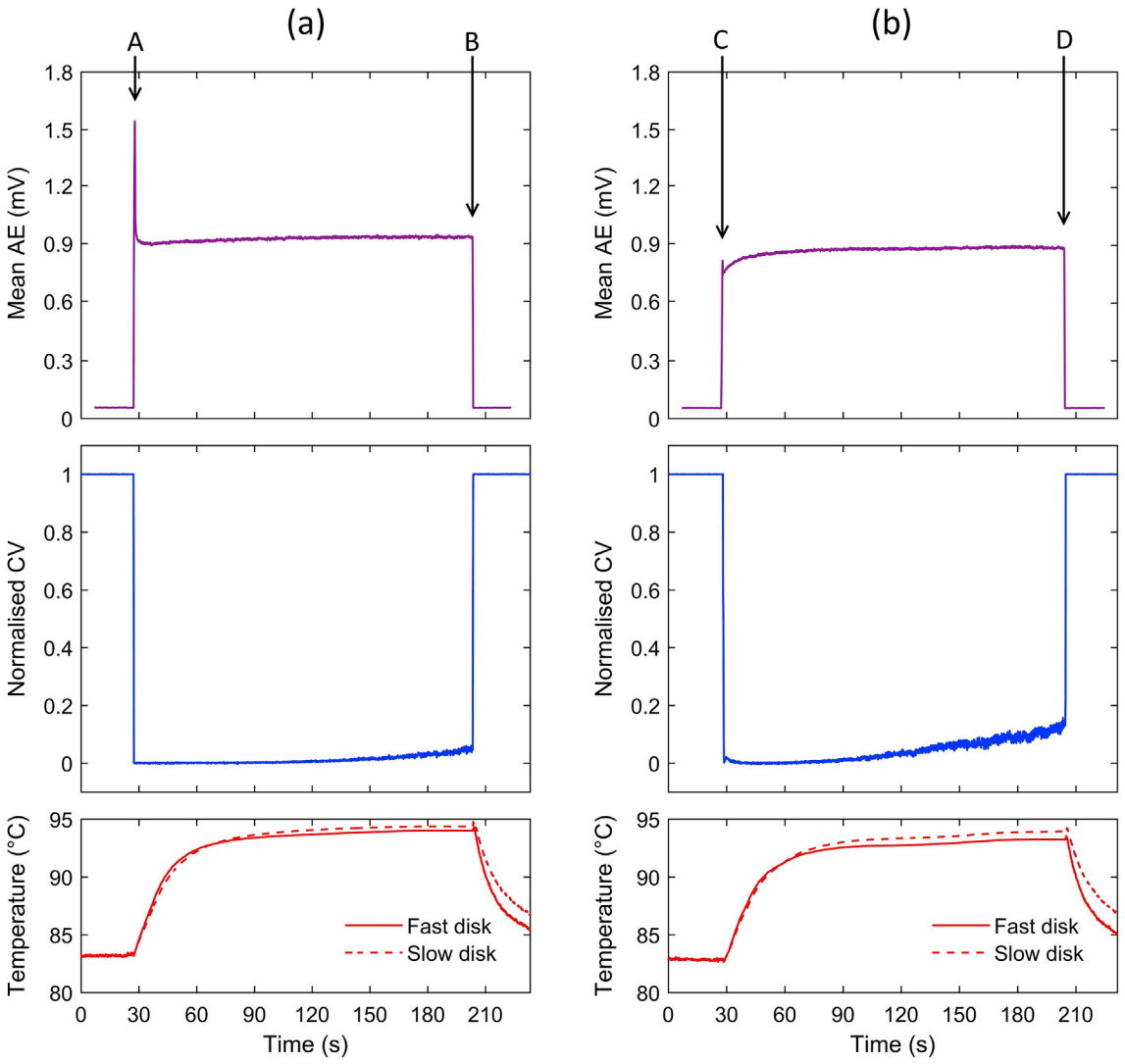

Fig. 7. AE, CV and the temperature data for (a) the first test stage, 0–3000 fast disk cycles and (b) the second test stage 3000–6000 fast disk cycles. Data for the unloaded periods preceding and following the test are also shown, with arrows A and C indicating the points of loading and B and D the points of unloading.

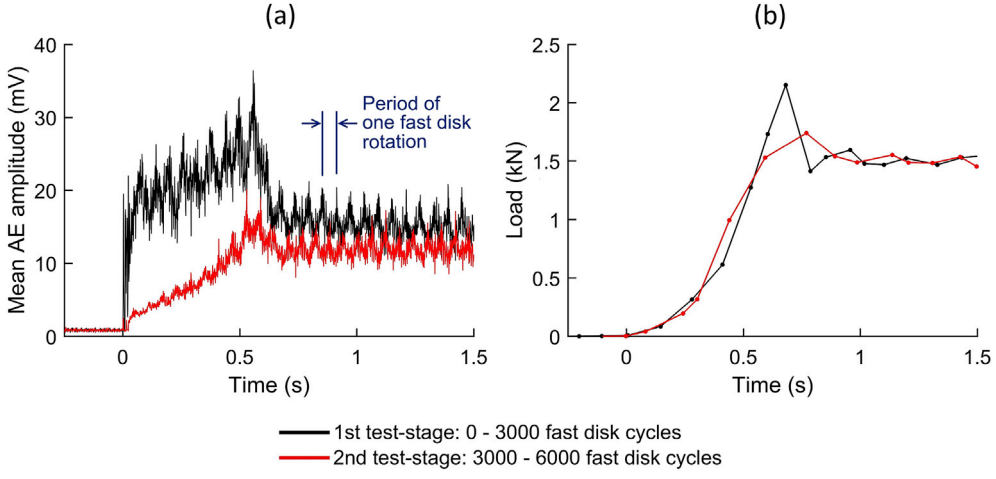

Fig. 8. Comparison of (a) AE and (b) load at the start of the first two test stages.

the first test stage.

The AE results from Fig. 7 indicate that the start of the test needs to be considered in greater detail. Fig. 8 presents the AE and load response at the start of the first two test stages, during the loading period. For this the mean AE was calculated using a narrow window having a width of 1.25 ms, equivalent to 7.5° of rotation of the fast disk. This results in

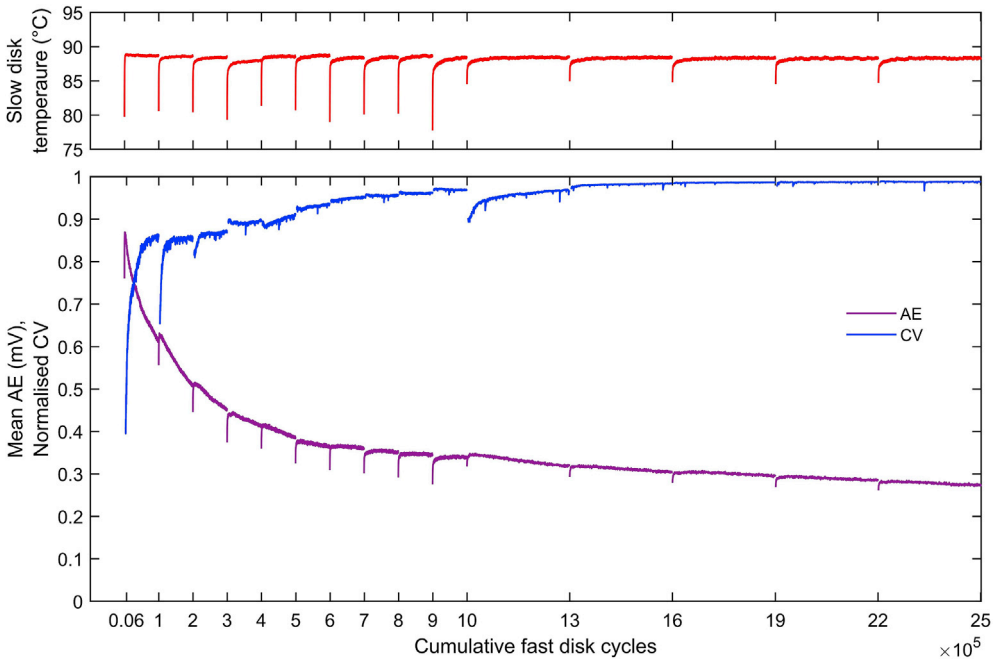

Fig. 9. AE, CV and temperature data for the micro-pitting experiment, test stages 3–18. The abscissa tick marks indicate the start/end of each test stage, i.e. the points at which the surface roughness of each disk was measured.

minimal temporal averaging with the effect that rotational frequencies are not filtered out as is the case for the wider window used in Fig. 7. (It should be noted that the scale of the mean AE amplitude is dependent of the window width which is why it differs between Figs. 7 and 8. As only relative changes in the AE are considered in this paper this is of little consequence). There are significant oscillations in the mean AE at the frequency of the fast disk rotation. These may be caused by one or more of the following cyclic affects: the AE sensor position relative to the contact; the slip ring connection; dynamic rotational loads, perhaps caused by load transmission error; and most intriguingly, any variation in the circumferential roughness of the disk affecting the amount of AE from the contact. Further testing would be required to quantify the contribution of each of these factors to the low frequency components of the AE signal.

Fig. 8 shows that the transient peak in the AE occurs within the period affected by loading transients so it is necessary to assess the implications of these. The sampled load was averaged over each fast disk rotation so the temporal resolution is not high but despite this it can be seen that at the start of both test stages there was a brief transient peak in the load which quickly settled. The transient peak at the start of the second stage appears to be of lower amplitude, this may have been the case or an artefact of the low sampling rate. It is known that AE is dependent on load so the peak in this must have contributed, at least partly, to the peak in the AE independent of the running-in process. Crucially however, the loading ramps during the first 0.5 s of each stage are similar whereas the AE responses are not. For the first stage there is a significant jump in amplitude followed by an increase to well above the subsequent steady state value, whereas for the second stage the jump is almost absent and the increase barely exceeds the subsequent steady state value. These differences are attributed to the presence of running-in in the first stage and its absence in the second, and support the conclusion that the running-in seen in these tests occurs very rapidly, in the first few cycles of operation. Indeed, this occurs in no more than two cycles of the complete set of asperity interactions and in only once cycle at the target load when the load ramp is considered.

It is interesting to compare the AE and CV measurements, which should both be sensitive to asperity contact levels. Fig. 7 shows that at the start of the first test-stage (A), the CV immediately drops to zero, its minimum, where it remains for most of the stage except towards the end when it begins to increase slightly. The extended period when the CV is at zero reveals one of the major limitations of this measurement technique: its low range. In practice the electrical resistance of a contact will become negligible with even a relatively small amount of direct asperity contact. At this point the CV will saturate at zero and will not measure any further increases in direct contact. This is why there is no transient reduction in CV equivalent to the peak in the AE results. For the second test stage the CV drops instantly to a low value before gradually decreasing to zero and then increasing in the latter half of the stage. The initial short decrease to zero mirrors that of the increase in AE and is attributed to temperature effects as discussed earlier. The gradual increase in the CV, for both test stages, appears to indicate that there is some continual reduction in direct asperity contact over the course of each. However there is no corresponding decrease in the AE amplitude which is to be expected from such behaviour. This may simply be due to the difference in sensitivities of the two measurement techniques. Although the CV has a narrow measurement range, it has great sensitivity within this range [24,28]. It is possible that the CV is responding to a change too slight to be detected in the AE signal. However, regardless of the AE results, the CV increases cannot represent the bulk of the running-in as this has been shown, by the roughness measurements, to have occurred predominantly in the first stage, whereas the increase in the CV is greater in the second stage. This suggests the presence of some unknown contact or measurement phenomenon affecting the CV independently of the amount of asperity contact. The comparison between AE and CV results shows the former to be more suitable for investigating running-in due to its superior range and consistency with the measured surface change.

6. Micro-pitting fatigue

In this section the AE measurements made in the micro-pitting fatigue test are discussed. Fig. 9 shows the mean AE measurements for the whole of this test, i.e. from the 6000th fast disk cycle onwards, together with the slow disk temperature and the CV. The abscissa tick positions indicate points at which the test was paused for a surface measurement and the start and end of each test stage. For clarity, data acquired during the unloaded period before and after each test stage is not presented.

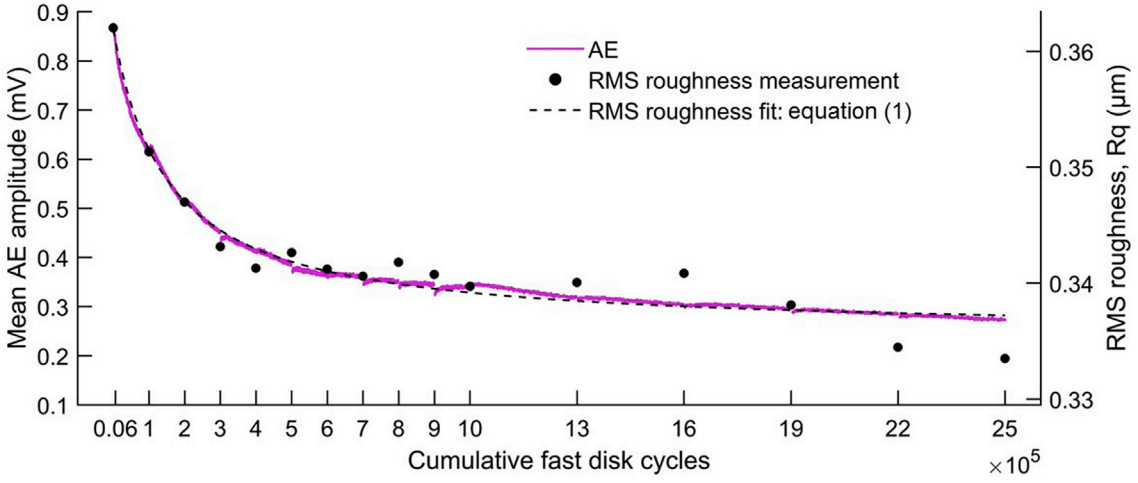

Fig. 10. Comparison of the change in the acoustic emission and the RMS roughness over the full micro-pitting test. The RMS values have been calculated using the measurements from both disks.

Additionally the intermittent sampling regime used during the fatigue test filters out the loading transients and thus none of the data presented in Fig. 9 are affected by these. There are however temperature transients caused by the resumption of frictional heating when the disks are reloaded at the start of each new test stage. The asymptotic temperature response is similar to that presented in Fig. 7 for running-in but due to the significantly longer duration of the fatigue test the initial steep rise appears as an instantaneous temperature jump at the start of each stage. The starting temperature for the last five and longer test-stages, from 10×10^5 cumulative fast disk cycles onwards, appears to be higher. This was not the case and it is an artifice caused by the change to a lower sampling frequency. As discussed for the running-in results a temperature increase causes a thinning of the oil film, causing the initial jump in the AE amplitude at the start of each test stage. During this transient the change in surface roughness, if measured, would have been negligible, so the change in AE is due to thermal effects reducing the film thickness. Although not the main subject of this paper it is worth noting that the transients reveal the high sensitivity of AE measurement to changes in the film thickness. Using a commonly used formula [29], the decrease in the predicted central film thickness, for an increase in contact temperature from 80 to 90 °C, is approximately 20% or in absolute terms 0.07 μm. There were also CV transients associated with the temperature jump, for clarity these have been cropped out of Fig. 9 by removing the first 3 min of CV data at the start of each test stage. Disregarding these transients, the contact temperature during the entire fatigue test remained within a range of 2.5 °C.

Post-processing parameters for the AE data were chosen so that the scales of Figs. 7 and 9 are comparable. It can therefore be seen that the AE at the start of fatigue testing was consistent with its value at the end of the running-in testing at just below 0.9 mV. After this there is a smooth asymptotic decrease in the AE to a value of under 0.3 mV. For the fatigue test, as opposed to the running-in, the relative duration of the starting transients is negligible and thus all contact parameters, except surface roughness, can be considered constant over the course of the test. The change in AE over the course of the test can therefore only be due to a change in surface roughness. This proves that the AE from the contact is dependent on the amount of asperity contact. This has been previously inferred from tests conducted by other researchers but the importance of the results presented here is that the surface roughness was the only variable. Commonly, speed and load variation are used to investigate different contact conditions, but as these are known to affect the AE independently of the amount of asperity contact [5] such experiments can be ambiguous and difficult to interpret. It is also interesting to note that the changes in AE are greater over the first stages. This corresponds to the increase in measured micropit depth which is significantly greater in the first section of the test than in the latter stages (Fig. 6).

The CV results in Fig. 9 broadly support those of the AE. There is a general increase in the CV to a value just under the maximum of one. The decrease in AE and increase in CV both indicate decreasing asperity contact which in this case can only be due to surface wear/micropitting, the presence of which has been confirmed by the roughness measurements. The high final CV value indicates that, by the end of the test, the surface roughness had reduced to the extent that the lubrication conditions were near full-film. Given this it is highly likely that, had the test been continued, it would have run for many millions more cycles with only negligible further surface wear. This supports the earlier assertion that micro-pitting fatigue was, in this case, a self-limiting process. It could be argued that since it resulted in an improvement in the contact conditions, i.e. less direct asperity contact, it could be viewed as a secondary phase of the running-in process rather than as damage.

Fig. 10 examines the relationship between the RMS roughness of the disks and the AE over the duration of the fatigue test. To produce this figure a rational function fit, Equation (1), for the RMS roughness was calculated using a non-linear least squares method.

$$y = \frac{ax + b}{x + c} \tag{1}$$

The ordinates of the AE and RMS roughness were then scaled and positioned so that the values of the roughness fit and the AE amplitude are at identical heights at the beginning and end of the test. For clarity the portions of the AE results affected by starting transients have been omitted. It can be seen that the results of the RMS roughness and AE measurements are in broad agreement with both having a similar asymptotic form. There is some significant uncertainty in the comparison but, perhaps unexpectedly, this is due to imprecision in the RMS roughness measurements rather than in the AE. It is likely that the difference in precision can be attributed to the difference in the effective sample size of each. The AE measurements effectively sampled the roughness of the entire contact path whereas the 2D profilometry measurements only sampled a small fraction of this. The problems of imprecision in the RMS roughness serve to highlight the relative ease with which suitably band-pass filtered AE measurements can be used to detect minute changes in the conditions of the surfaces of a lubricated contact.

There is considerable interest in the possibility that wear mechanisms have specific AE signatures, usually in terms of their frequency, that can be used to distinguish them from the AE ‘noise’ inherent in rotating machinery [15,16]. The utility of such a signature is clear: it would allow incipient damage to be detected that would other-wise be drowned out

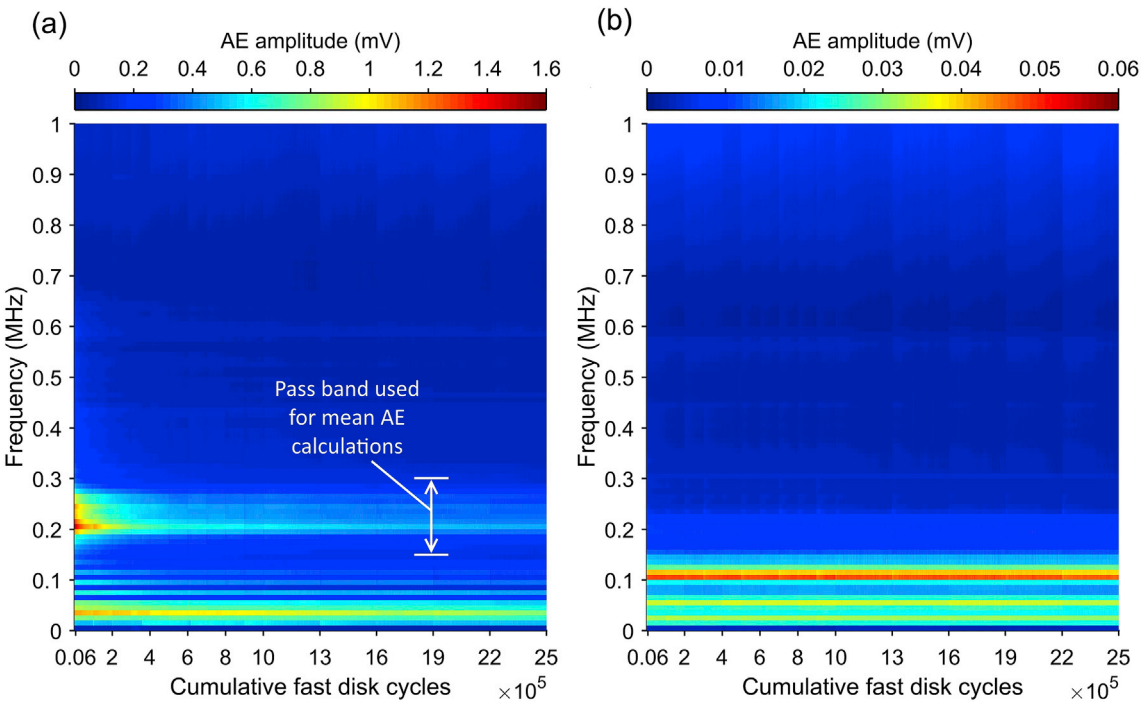

Fig. 11. The spectral distribution of the AE over the course of the micro-pitting test for a) the fast disk transducer and b) the bearing housing transducer. For clarity the AE amplitude is presented as the average of 10 kHz wide frequency bins.

by general operating noise. It is worth then considering if the micro-pitting induced in this testing had some AE signature that distinguishes it from the bulk signal. Take first, the premise that the formation of a micro-pit causes a transient increase in the broadband AE amplitude, the mostly likely cause of which would be material fracture during crack growth. If this were the case then in periods of significant micro-pit formation the AE amplitude might be expected to deviate to levels above that expected from direct asperity interaction alone. The results of the fatigue test presented thus far show no evidence of this. It has been shown that the majority of micro-pitting occurred in the period between 6000 and 2×10^5 fast disk cycles so this is the expected location of any deviation. However, as Fig. 10 shows, there is a good correlation between the AE and the RMS roughness during this period. This implies that any broadband AE from micro-pit formation was insignificant compared to that from general asperity interaction, and that in this experiment the AE is sensitive to changes in asperity interaction caused by micropit formation, rather than directly to the crack-growth mechanisms themselves. The second premise is that the frequency content of the AE from micro-pit formation is different to that from asperity interaction.

Fig. 11 shows the spectral distribution of the AE over the duration of the fatigue test. The frequency band of 0.15–0.3 MHz used to calculate the mean AE amplitude results in this paper is marked. It can be seen that for the fast disk transducer, Fig. 11(a), there is significant and variable activity within this range. In comparison, for the bearing housing transducer, Fig. 11(b), there is negligible activity within this range, as indicated by the different colour scale used in this figure. This demonstrates that the AE measured within this range is from the test contact and not from potential sources of noise such as the support bearings. The fast disk transducer shows that the amplitude of frequency components above 0.3 MHz is barely above that of the background level and even when examined at a finer resolution there are no patterns in the distribution that can plausibly be related to micro-pit formation. However, as with all AE measurements, the frequency components of signals are not only related to the source mechanism, but also to the signal transmission path and sensor sensitivity. Below 0.15 MHz there are bands of significant amplitude in the signal from the fast disk transducer but there is relatively little variation in the amplitude of these over the course of the test and so it is highly unlikely that they are related to micropit formation. Additionally the bearing housing transducer also shows significant activity in this region which suggests that it is susceptible to noise and thus of little use for investigating asperity interactions. The results from the fatigue test have shown that if micro-pitting formation does have a distinct AE signature it is extremely subtle, and may only be revealed by further analysis using more complex techniques which examine changes in the AE signal over much shorter timescales, for example resolved in terms of angular position during individual disk rotations. It may be that advanced analysis techniques [16] could uncover it, but it is more likely that if such a signature does exist, it is indistinguishable from the background AE caused by asperity interaction. However, it cannot be denied that this work has demonstrated the sensitivity of AE to changes in mixed lubrication conditions due to surface topography modifications caused by micropitting and micro-wear mechanisms.

7. Conclusions

This work has shown that Acoustic Emission is a sensitive tool for studying subtle changes in mixed lubrication conditions during both the running-in and micropitting processes. Detailed measurements of the evolution of surface topography have shown that running-in is a rapid process whereby prominent asperities are flattened during the first few cycles of operation. This is reinforced by consideration of the AE signals recorded during the initial operation of the twin disk test rig. During subsequent operation of the run-in surfaces, the formation of micropits was quantified using in-situ relocation profilometry. AE signals recorded during the micropitting test were strongly related to changes in surface topography, with a close correlation between AE signals and RMS surface roughness. However, examination of the frequency content of the AE signals did not show characteristic features related to the crack-growth and fracture mechanisms at work during the formation of micropits. Rather, this research demonstrates that AE is highly sensitive to the *resulting* changes in asperity interaction under mixed lubrication conditions, due to micropitting. In general, AE was found to be more sensitive to mixed lubrication conditions than the contact voltage technique, as the AE was still able to discern subtle changes in conditions after the contact

voltage measurement had saturated. AE is therefore proposed as a useful tool for the experimental study of mixed lubrication conditions, which has the potential to offer detailed insight into contact behaviour under realistic operating conditions.

Data access statement

Information on how to access the data that supports the results presented in this article can be found in the Cardiff University data catalogue at https://doi.org/10.17035/d.2016.0008118727.

Acknowledgements

The authors wish to acknowledge the support of EPSRC Grant reference EP/L021757/1 which facilitated this work in part.

References

[1] Loutas TH, Sotiriades G, Kalaitzoglou I, Kostopoulos V. Condition monitoring of a single-stage gearbox with artificially induced gear cracks utilising on-line vibration and acoustic emission measurements. Appl Acoust 2009;70:1148–59.
[2] Loutas TH, Roulias D, Pauly E, Kostopoulos V. The combined use of vibration, acoustic emission and oil debris on-line monitoring towards a more effective condition monitoring of rotating machinery. Mech Syst Signal Process 2011;25:1339–52.
[3] Elforjani M, Mba D. Accelerated natural fault diagnosis in slow speed bearings with Acoustic Emission. Eng Facture Mech 2010;77:112–27.
[4] Schnabel S, Marklund P, Larsson R, Golling S. The detection of plastic deformation in rolling element bearings by acoustic emission. Tribol Int 2017;110:209–15.
[5] Cockerill A, Clarke A, Pullin R, Bradshaw T, Cole P, Holford KM. Determination of rolling element bearing condition via acoustic emission. Proc IMechE Part J J Eng Tribol 2016;230(11):1377–88.
[6] Douglas RM, Steel JA, Reuben RL. A study of the tribological behaviour of piston ring/cylinder liner interaction in diesel engines using acoustic emission. Tribol Int 2006;39:1634–42.
[7] Hase A, Mishina H, Wada M. Correlation between features of acoustic emission signals and mechanical wear mechanisms. Wear 2012;292–293:144–50.
[8] Price ED, Lees AW, Friswell MI. Detection of severe sliding and pitting fatigue wear regimes through the use of broadband acoustic emission. Proc IMechE Part J J Eng Tribol 2005;219:85–98.
[9] Saeidi F, Shevchik SA, Wasmer K. Automatic detection of scuffing using acoustic emission. Tribol Int 2016;94:112–7.
[10] Wang L, Wood RJK. Acoustic emissions from lubricated hybrid contacts. Tribol Int 2009;42:1629–37.
[11] Toutountzakis T, Mba D. Observations of acoustic emission activity during gear defect diagnosis. NDT&E Int 2003;36:471–7.
[12] Toutountzakis T, Keong Tan C, Mba D. Application of acoustic emission to seeded gear fault detection. NDT&E Int 2005;38:27–36.
[13] Singh A, Houser DR, Vijayakar S. Detecting gear tooth breakage using acoustic emission: a feasibility and sensor placement study. Trans ASME J Mech Des 1999;121:587–93.
[14] Crivelli D, McCrory J, Miccoli S, Pullin R, Clarke A. Gear tooth root fatigue test monitoring with continuous acoustic emission: advanced signal processing techniques for detection of incipient failure. Struct Health Monit 2017. https://doi.org/10.1177/1475921717700567.
[15] Scheer C, Reimche W, Bach F-W. Early fault detection at gear units by acoustic emission and wavelet analysis. J Acoust Emiss 2007;25:331–40.
[16] Wirtz SF, Beganovic N, Tenberge P, Soffker D, Frequency-based damage detection of spur gear using wavelet analysis, presented at 8th European Workshop on Structural Health Monitoring (EWSHM 2016), 5–8 July 2016, Bilbao, Spain.
[17] Barrueot Novoa A, Molina Vicuna C. New aspects concerning the generation of acoustic emissions in spur gears, the influence of operating conditions and gear defects in planetary gearboxes. Insight 2016;58(1):18–27.
[18] Molina Vicuna C. Effects of operating conditions on the Acoustic Emissions (AE) from planetary gearboxes. Appl Acoust 2014;77:150–8.
[19] Raja Hamzah RI, Mba D. Acoustic emission and specific film thickness for operating spur gears. Trans ASME J Tribol 2007;129:860–7.
[20] Raja Hamzah RI, Mba D. The influence of operating condition on acoustic emission (AE) generation during meshing of helical and spur gear. Tribol Int 2009;42:3–14.
[21] Tan CK, Mba D. Identification of the acoustic emission source during a comparative study on diagnosis of a spur gearbox. Tribol Int 2005;38:469–80.
[22] Tan CK, Mba D. Correlation between acoustic emission activity and asperity contact during meshing of spur gears under partial elastohydrodynamic lubrication. Tribol Lett 2005;20(1):63–7.
[23] Clarke A, Weeks IJJ, Snidle RW, Evans HP. Running-in and micropitting behaviour of steel surfaces under mixed lubrication conditions. Tribol Int 2016;101:59–68.
[24] Clarke A, Weeks IJJ, Snidle RW, Evans HP. An investigation into mixed lubrication conditions using electrical contact resistance techniques. Tribol Int 2016;93:709–16.
[25] Patching MJ, Kweh CC, Evans HP, Snidle RW. Conditions for scuffing failure of ground and superfinished steel disks at high sliding speeds using a gas turbine engine oil. Trans ASME J Tribol 1995;117(3):482–9.
[26] Ministry of Defence Defence Standard 91-74 Lubricating Oil. Steam turbine and gear, extreme pressure joint service designation. 2000. OEP-80, no. 2.
[27] Jamari J. Running-in of rolling contacts. PhD Thesis. The Netherlands: University of Twente; 2006.
[28] Guangteng G, Olver A, Spikes HA. Contact resistance measurements in mixed lubrication, in: the advancing frontier of engineering tribology. In: Proceedings of the 1999 STLE/ASME H.S. Cheng tribology surveillance; 1999. p64.
[29] Chittenden R, Downson D, Dunn J, Taylor C. A theoretical analysis of the isothermal elastohydrodynamic lubrication of concentrated contacts II: general case, with lubricant entrainment along either principal axis of the Hertzian contact ellipse or at some intermediate angle. Proc R Soc Lond A 1969;313:509–29.